Desalination and Water Treatment
www.deswater.com

doi: 10.5004/dwt.2020.25052

180 (2020) 360–369
March

Photocatalytic activity of GO-doped bismuth-based photocatalyst for Methyl Orange decolorization under visible light irradiation

A. Rahimi[a], M. Hasani Zonoozi[a,*], R. Rahimi[b], B. Zahabiyoun[a]

[a]*Department of Civil Engineering, Iran University of Science and Technology (IUST), Narmak, Tehran 16846-13114, Iran, Tel. +98-21-7322-8194/+98-912-2898341/+98-21-7322-0399; Fax: +98-21-77240398; emails: mhzonoozi@iust.ac.ir/ maryamzonooz@yahoo.com (M. Hasani Zonoozi), a_rahimi@alumni.iust.ac.ir (A. Rahimi), bagher@iust.ac.ir (B. Zahabiyoun)*
[b]*Department of Chemistry, Iran University of Science and Technology (IUST), Narmak, Tehran 16846-13114, Iran, Tel. +98-21-7749-1208, email: rahimi_rah@iust.ac.ir*

Received 17 December 2018; Accepted 17 October 2019

ABSTRACT

It was aimed to investigate the photocatalytic activity of GO-doped $BiVO_4$ nanocomposite (m-BVG) as novel visible-light bismuth-based photocatalyst for decolorization of a selected azo dye (methyl orange, MO) from water. According to the obtained results, the synthesized m-BVG represented a better photocatalytic performance and exhibited higher decolorization rate and efficiency at any given time of the test in comparison with the synthesized $BiVO_4$ nanoparticles. Owing to GO electrical conductivity, reduction of the recombination rate of electron–hole pairs resulted in more efficient performance for the m-BVG. The solution permeability to light, which is a function of both m-BVG dosage and dye concentration, was distinguished as a predominant controlling factor of the decolorization efficiency. Applying H_2O_2 (at the content of 2 wt.%) as an external electron acceptor in association with m-BVG, dramatically enhanced the decolorization rate. Presence of H_2O_2 eliminated the necessity of going through the long pre-required pathway (comprising of six successive reactions) for the subsequent OH^- generating reactions. Under this circumstance and owing to the synergistic performance of H_2O_2/m-BVG composite, around 98% MO decolorization was achieved over only 10 min of irradiation while it lasted about 330 and 60 min for m-BVG and H_2O_2, orderly, to gain the same decolorization efficiency when they were used individually.

Keywords: GO-doped $BiVO_4$; Photocatalytic activity; H_2O_2; Methyl orange; Decolorization

1. Introduction

Dyes are one of the largest and most important groups of organic compounds used in several industries such as textile, plastics, cosmetics, food, papermaking and printing. Due to large volumes of water consumption in the different sections of these industries, remarkable amounts of colored wastewaters are generated annually [1]. Considerable environmental and health hazards have been attributed to synthetic dyes. Discharge of untreated dye-containing effluents in aqueous ecosystems is aesthetically undesirable. It also impedes the sunlight penetration into aqueous environment which consequently retards the photosynthetic activity and inhibits the biota growth [2]. Acute toxic effects on aquatic plants and long-term environmental problems have also been reported for the dye compounds [3]. Azo dyes constitute the largest part of synthetic dyes. According to the reports around 50% of the commercially available dyes are of this type. They are characterized by at least one nitrogen to nitrogen double bond (N=N), which is called azo group, in their chemical structure. Many azo dyes have been proved to be toxic and carcinogenic for the living organisms [2,4,5]. Therefore,

* Corresponding author.

it is necessary to remove these organic compounds from textile wastewaters before releasing them into natural water bodies.

Recently, intensive researches have been performed regarding the azo dye removal from effluents by using advanced oxidation processes (AOPs). In the mentioned processes, strong oxidants such as free hydroxyl radical ($OH^{\cdot}$) result in complete mineralization of organic pollutants. Heterogeneous photocatalysis is one of the robust techniques among the various in the category of AOPs. No waste disposal problem and facile operating conditions have been accounted as some advantages of the photocatalytic process [4,6,7]. The process is mostly believed to be based on migration of valence electrons from the valence band to the conduction band and the consequent generation of electron–hole pair on the catalyst surface under irradiation of ultraviolet or visible light as energy source. This procedure induces the photocatalytic water oxidation process during which the superoxide radical anions ($O_2^{\bullet-}$) and free reactive OH radicals are produced. These photogenerated reactive species have a strong tendency to interact with the organic substances and destroy them in aqueous medium [6–10].

Various solid semiconductors such as metal oxides (TiO_2, ZnO, CeO_2, ZrO_2, WO_3, V_2O_5, Fe_2O_3, etc.) have been intensively used as catalyst in heterogeneous photocatalysis [7]. In order to excite the valence electron, the irradiation wavelengths energy should be larger than the band gap energy ($hv \geq E_g$) of the catalyst material, and because of this, the required energy level will directly depend upon the selected metal oxide [6].

Until present, TiO_2 and ZnO have been frequently investigated for many photocatalytic reactions [11,12]. However, due to their wide band gap of 3.2 eV, their application is limited to the ultraviolet light which represents only 4% of the solar light as a reproducible energy source [7,9,11–13]. Valuable efforts have been made to produce and introduce new compositions of semi-conductive materials with narrow band gaps so that the photocatalysis procedure could be performed under irradiation of wavelengths with lower energy levels such as visible and sunlight [7,9,11,12,14,15]. In this regard, bismuth-based semiconductors have gained researchers' attention because of their interesting physiochemical properties, especially the highly visible-light-induced photocatalytic activity [16–19]. As an outstanding example, the monoclinic bismuth vanadate ($BiVO_4$) has been extensively investigated because of its comparative narrow band gap (2.4 eV) and intrinsic photocatalytic activity under visible light irradiation [9,11,13,19,20]. However, the photocatalytic activity of bismuth-based semiconductors, pure $BiVO_4$ in particular, has been reported to be restricted by the high recombination rate of photogenerated electron–hole pairs and poor surface adsorptive performance [11,14,16]. As reported by some researchers, doping with different metal (e.g., Au Co, Ag, Ni) and nonmetal elements (e.g., N, F, B) could enhance the $BiVO_4$ photocatalytic activity under visible light irradiation through facilitating the charge separation (e^-/h^+) and reducing the electron–hole pairs recombination rate [11,14,20,21–23].

Recently, reduced graphene oxide (GO), as a dopant to synthesize GO-metal oxide hybrid structures, has gained a lot of attention with the aim of promoting the photocatalytic activity. Owing to the excellent electrical conductivity and high surface area, GO can serve as an electron acceptor, expedite the electron transfer and prevent the recombination of the charge carriers [19,24,25]. To the best of our knowledge, there are very few reports [19,26] on the synthesis and photocatalytic properties of GO-doped $BiVO_4$ composite (BVG). In the present work, the authors attempted to investigate the photocatalytic activity of BVG as novel visible-light bismuth-based photocatalyst in order to decolorize the selected azo dye (methyl orange, MO) from water. For this purpose, GO, $BiVO_4$ and BVG composites were synthesized and examined. It was also focused on the effect of H_2O_2 addition as an external electron acceptor on BVG performance. The possible mechanisms of the photocatalytic reactions were also discussed in details.

2. Experimental setup

2.1. Materials and instrumentation

Ethanol (purity of 99%), hydrogen peroxide (35%, v/v), graphite powder (300 mesh, purity of 99.99%), nitric acid (65%, v/v), sodium hydroxide, ammonium metavanadate (NH_4VO_3, purity of 99%), bismuth (III) nitrate ($Bi(NO_3)_3{\cdot}5H_2O$, purity of 98%) and sulfuric acid (purity of 95%–97%) were purchased from Merck (Germany). The azo dye methyl orange (MO, λ_{max} of 504 nm and purity of 99.9%) was supplied by Sigma-Aldrich company.

A Shimadzu UV-1700 spectrophotometer (Japan) was applied in order to record the UV-visible spectra of the dye-containing samples. The decolorization efficiencies were determined by using the previously developed absorbance–concentration curve of the dye at 504 nm. As the visible light source, a 40-W LED lamp was utilized. The structural morphology observation was performed by a field emission scanning electron microscope (SEM; ZEISS Sigma 500 VP FE-SEM, Germany). To analyze the chemical composition of the synthesized materials, an Oxford Instruments Energy-Dispersive Spectroscopy (made in UK) was applied. The micro-structure and crystallinity of the synthesized materials were studied by using of a Philips PW1730 X-Pert diffractometer (Netherlands) using Cu Kα radiation in a 2θ range of 10°–80°. Oven (Memmert-UFP400, Germany), centrifuge (Wisespin-CF-10, Korea) and ultrasonication instrument (Elma-S60H, Germany) were also used during the experimental period.

2.2. Synthesis of materials

Graphene oxide (GO) was synthesized by the Hummers' method [27] and exfoliated under ultrasonication to give a brown uniform dispersion. To synthesize the $BiVO_4$ nanoparticles, the hydrothermal method described by Karunakaran et al. [28] was used. A facile one-step hydrothermal method was applied to synthesize the grapheme-doped $BiVO_4$ (BVG) nanocomposite. As the first step, 485 mg of bismuth (III) nitrate powder was dissolved in 20 mL of 1 M HNO_3 by stirring at room temperature for 30 min to produce $Bi(NO_3)_3$ solution (solution A). After that, 1.4 mg of GO was dissolved in solution A under ultrasound irradiation (solution B). Alkaline solution of NH_4VO_3 (solution C) was prepared by

dissolving 117 mg (1 mmol) of NH_4VO_3 in 20 mL of 0.05 M NaOH by stirring at room temperature for 30 min. Then, solution C was added drop wise to solution B while stirring to get a clear solution. The resultant was transferred to a 100 mL Teflon-lined stainless steel autoclave, sealed and heated at 120°C for 24 h under autogeneous pressure and allowed to cool to room temperature. The obtained samples were washed with deionized distilled water and pure ethanol orderly and then allowed to dry at room temperature to get the final product. At one stage of the study, the modified version of BVG (m-BVG) was produced by increasing the heating temperature to 160°C.

2.3. Dark adsorption and photocatalytic reaction experiments

Dark adsorption and photocatalytic activity of synthesized materials were evaluated by using of 50 mL samples of methyl orange (MO) solution with 10 mg/L concentration under dark condition (the first 30 min of each experiment) and visible LED light irradiation, respectively. All experiments were carried out at 25°C in a 250 mL water-jacketed Pyrex flask as the container for the reactions. The mixture was stirred by using a magnet stirrer during each experiment. A 40-W LED lamp was utilized as the visible light source. pH adjustment was performed by a CORNING pH meter model 140. The samples were centrifuged before measuring the dye concentration.

3. Result and discussions

3.1. Crystal structure of synthesized materials

The structure of the synthesized materials was analyzed by SEM images, X-ray diffraction (XRD) pattern and energy dispersive X-ray spectroscopy (EDX) pattern. The SEM images of $BiVO_4$ are shown in Figs. 1a and b. As seen, the particles have an irregular amorphous structure. This is consistent with the results of the previous studies [9].

According to the EDX pattern presented in Fig. 1c, the obtained weight ratios of the Bi, O and V elements in the composite structure were compatible with the theoretical values in the $BiVO_4$ formula (i.e., 64%, 20% and 16%, respectively). This verifies the successful formation of $BiVO_4$ composite. The XRD pattern shown in Fig. 1d exhibits obvious peaks at $2\theta = 18.9°$, 28.9°, 30.5°, 34.7°, 39.9°, 42.3°, 45.8°, 47.1°, 50.1°, 53.1° and 58.4° which are those of monoclinic $BiVO_4$ structure (JCPDS 14-0688 standard card).

Graphene oxide was successfully prepared by the Hummers' method. The SEM images showed a sheet-like morphology for the synthesized GO (Fig. 2). The XRD patterns exhibited the 2θ of 26.1° and 9.2° for natural graphite powder and GO, respectively, which have been previously presented in a work performed by Rahimi et al. [8].

The SEM images of the synthesized GO-doped $BiVO_4$ (m-BVG) are shown in Fig. 3. As can be drawn from the figure, the morphology of the m-BVG is entirely different from

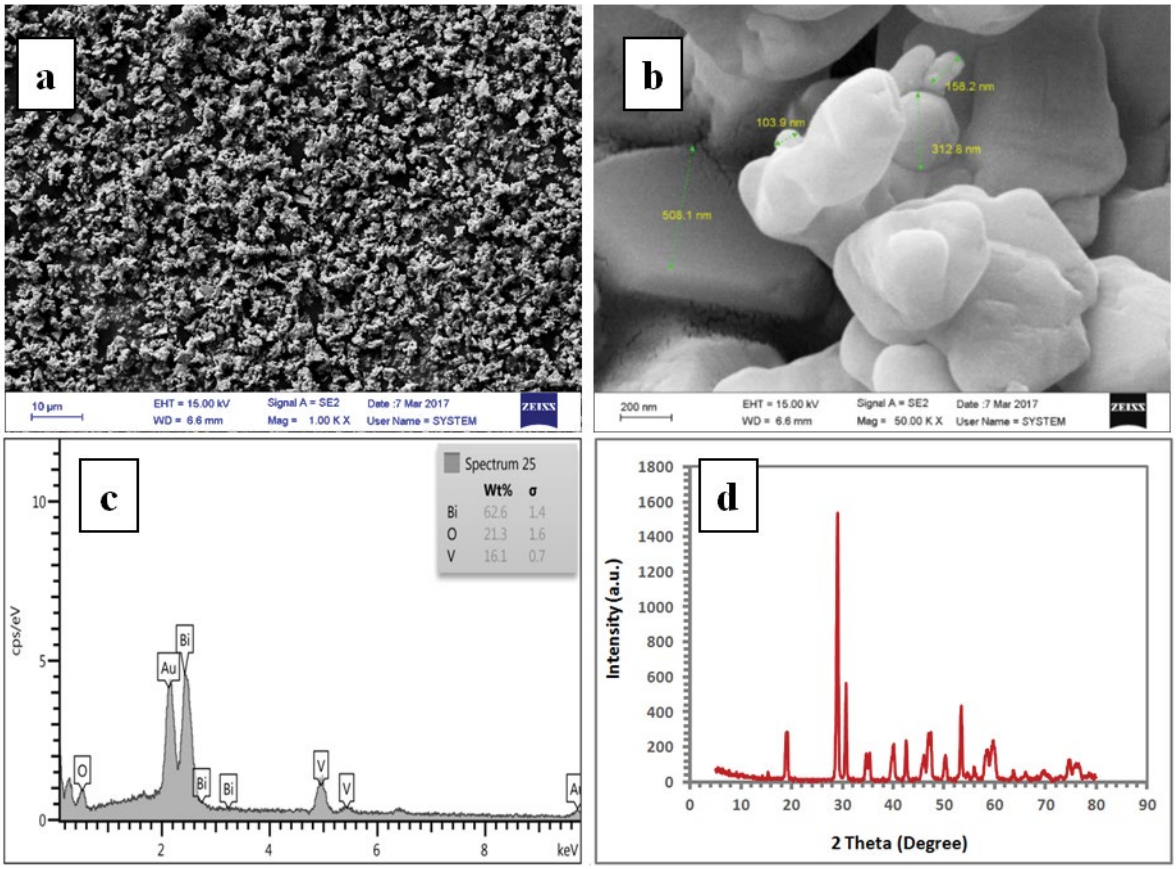

Fig. 1. (a and b) SEM images, (c) EDX spectrum and (d) XRD pattern of the synthesized $BiVO_4$.

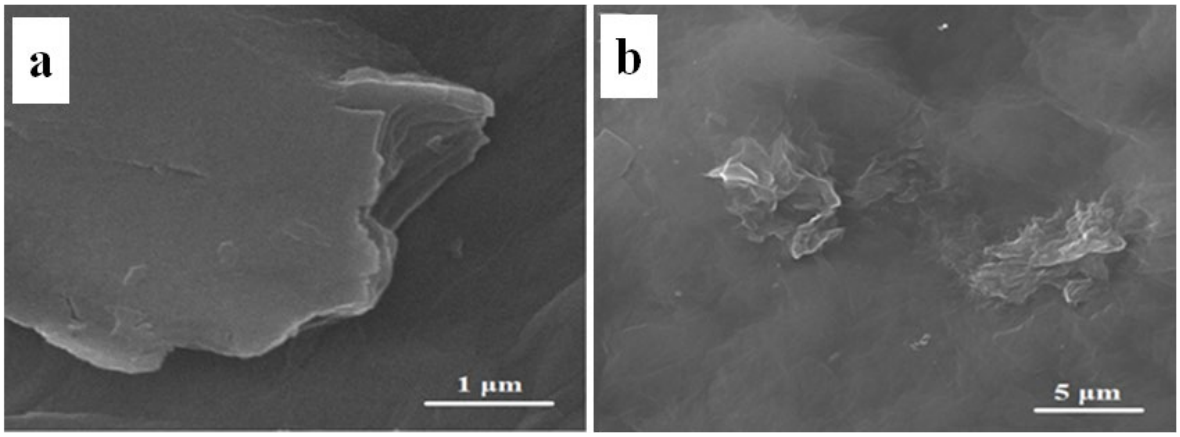

Fig. 2. SEM images of the synthesized GO.

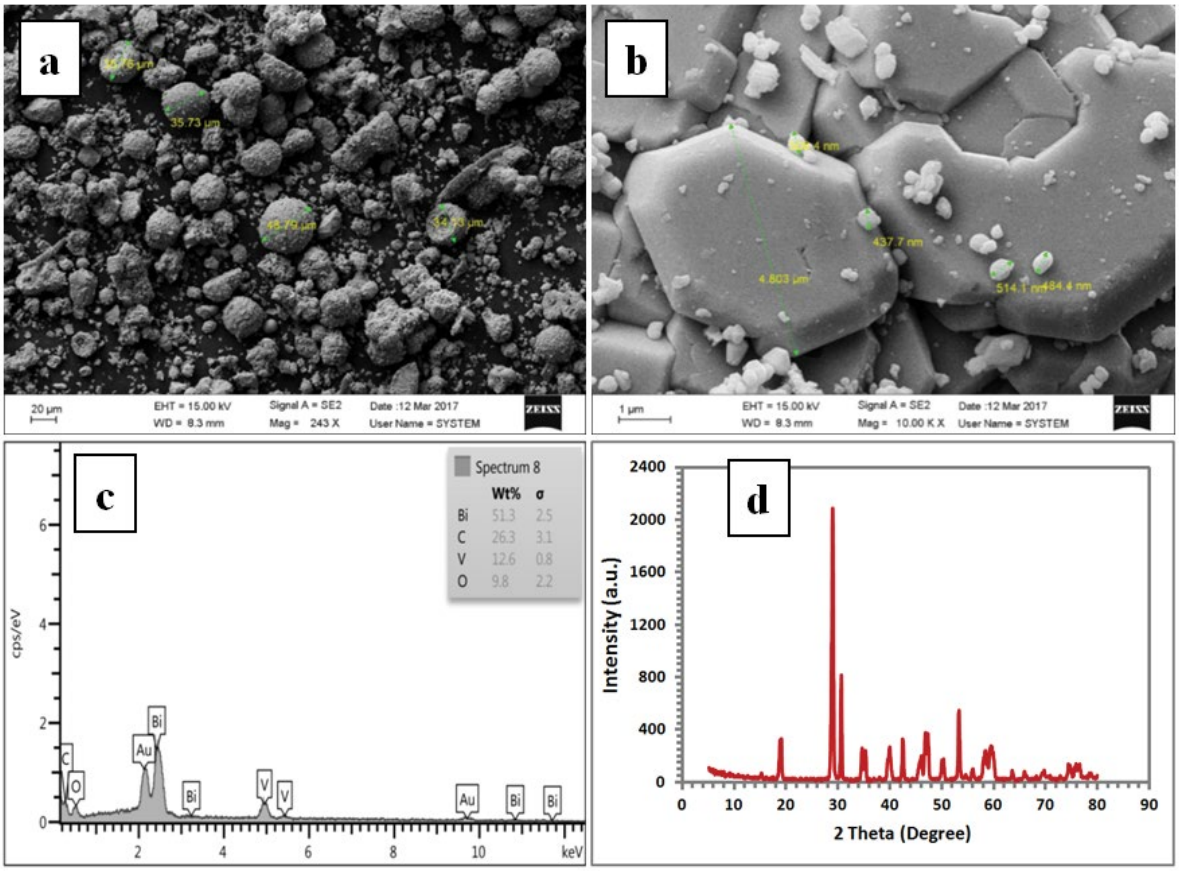

Fig. 3. (a and b) SEM images, (c) EDX spectrum and (d) XRD pattern of the synthesized m-BVG.

the sheet-like morphology of GO and the previous irregular structure of $BiVO_4$ nanoparticles. The main structure of the BVG nanocomposite comprises the spherical particles coated with the scattered pure $BiVO_4$ nanoparticles. According to the EDX analysis results, the synthesized BVG particles were composed of Bi, V, O and C atoms that the latter one was originated from GO. The BVG nanocomposites showed a similar XRD pattern to the pure $BiVO_4$. Graphene diffraction peaks are not observed in the BVG nanocomposites. Rahimi et al. [8], who observed similar XRD patterns for TiO_2 and TiO_2-graphene nanocomposites, described this by the low amount and the relatively low diffraction intensity of the graphene.

3.2. Decolorization performance of the synthesized materials

3.2.1. Adsorption on GO

GO with a dosage of 1,000 mg/L was added to 50 mL of 10 ppm MO solution at pH of 3. This pH was chosen as an

appropriate pH according to some pretests. The first 30 min of the reaction was performed under dark condition and after that, the LED light irradiation was used as visible light source. According to the obtained results (Fig. 4), light irradiation had no effect on the decolorization performance of the GO since the decolorizarion rate under dark adsorption was obviously high and it did not improve under LED light irradiation following the dark adsorption. This indicates that adsorption was the essential decolorization mechanism of the GO. It is notable that the decolorization rate decreased mainly within two steps over the entire time of the test. The slight decrease of the decolorization rate at the first step (step 1 in the figure) was most probably due to the rapid occupation of adsorption sites of GO sheets by MO molecules. At the second step (step 2), decreasing of the decolorization rate was caused by both the extreme reduction of the remaining available adsorption sites on GO sheets and the very low remaining dye concentration which led to insufficient collisions between the dye molecules and the GO nanoparticles. Peng et al. [29] who reviewed the heavy metal ions adsorption by GO have accounted the decrease of the driving force between the positively charged heavy metal ions and negatively charged GO sheets as a reason for falling rate of the adsorption over time. However, this cannot be the case for the MO molecules and GO particles since they are both negatively charged in aqueous environment. At the last 30 min of the test (i.e., after 330 min), the decolorization efficiency reached more than 80% and the adsorption–desorption equilibrium between the dye and the surface of the GO sheets was achieved.

3.2.2. Decolorization with $BiVO_4$, BVG and m-BVG

The decolorization performance of $BiVO_4$, and BVG nanoparticles at a dosage of 1,000 mg/L was examined separately by keeping the same reaction conditions described in section 3.2.1. The obtained results are depicted in Fig. 5. As seen in the figure, $BiVO_4$ and BVG had a very similar trend for the MO decolorization. They both exhibited negligible decolorization efficiency during the dark condition which indicates their low adsorption capability. After that, by irradiation of the visible light, the decolorization rate of both $BiVO_4$ and BVG increased up to an almost steady state in a short span. This trend was entirely different from that observed for GO. It is noteworthy that when testing with GO, a significant decrease in decolorzation rate was occurred as the C/C_0 reached about 0.4 (the 90th min); while during the test with $BiVO_4$ and BVG, the reduction of the decolorization rate was very moderate even at the C/C_0 of 0.2 (the 330th min). This can be attributed to the strong photocatalytic activity of both $BiVO_4$ and BVG which let them to perform less dependent on the dye concentration.

Formation of free radicals as a consequence of the light irradiation and the subsequent valence electron excitation had the main role in the increasing of the decolorization rate in the middle of the test time. No significant difference was observed between the decolorization performance of $BiVO_4$ and BVG so that a final decolorization efficiency of around 80% was obtained for both of them. This could be due to the improper doping of $BiVO_4$ on the GO sheets. For this reason, in the next step of the study, the modified version of BVG (m-BVG) was produced and examined for its decolorization performance.

The m-BVG showed negligible decolorization during the dark condition. After the light irradiation, the decolorization rate increased and stayed at an almost constant value until the end of the test despite that the remained dye concentration was very low. This was almost the same trend previously seen for $BiVO_4$ and BVG. As represented in Fig. 5, when m-BVG was used, the decolorization efficiency of 80% was obtained at the 240th min of the test which was about 2 h earlier in comparison with the test conducted by BVG and $BiVO_4$. Besides, at the end of the test, the decolorization efficiency using m-BVG reached about 100%. Considering the higher decolorization rate of m-BVG in comparison with both $BiVO_4$ and BVG, it seems that the former was benefitted from a better photocatalytic performance than the latter ones. This illustrates the outstanding electrical conductivity of GO that helped to reduce the recombination rate of electron–hole pairs in m-BVG compared with $BiVO_4$. The result also indicates that synthesis of graphene-supported $BiVO_4$ at 160°C better enhanced the photocatalytic activity compared with synthesis at 120°C. Xu et al. [30], and Hsieh and Ting [24], who investigated the photocatalytic activity of a ZnO/rGO (reduced GO) and Cu-ZnO/rGO, explained that the electron–hole recombination was reduced because of the role of the GO as an electron collector and transporter. Shan et al. [19] who synthesized $BiVO_4$/

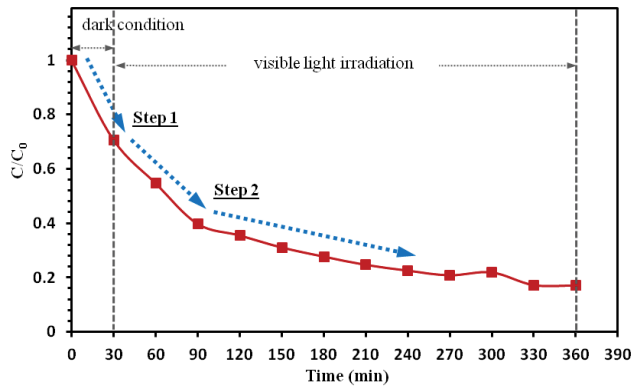

Fig. 4. Decolorization performance of GO.

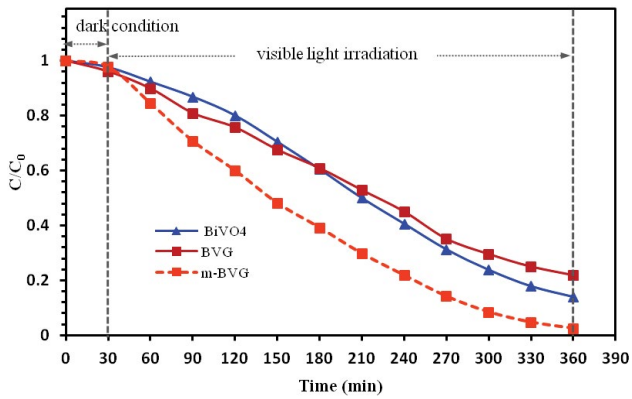

Fig. 5. Decolorization performance of $BiVO_4$, BVG and m-BVG.

rGO composite with different contents of GO described that using pure $BiVO_4$, the decolorization rate of Methylene Blue (MB) solution was only 25% in 360 min while it ran up to 80% for $BiVO_4$/rGO composite with 0.018 g content of GO. They also explained that increase in the GO content led to deterioration of the catalytic performance and concluded that suitable GO content is crucial for optimizing the $BiVO_4$/GO photocatalytic activity.

3.2.3. Effect of m-BVG dosage

To evaluate the effect of m-BVG dosage on decolorization performance, different amounts of m-BVG were dosed into the dye-containing samples. Fig. 6 shows the final decolorization performance of different m-BVG dosages. According to the results, with increasing the m-BVG amount from 200 to 1,000 mg/L, the final decolorization efficiency significantly increased from 40% to around 100% color removal. Further increase, particularly beyond 1,400 mg/L, resulted in a slight decrease in the decolorization efficiency. Dhatshanamurthi et al. [2] and Sathishkumar et al. [31] observed similar trends for photocatalytic decolorization using ZnO and CuO-ZnO nanoparticles, respectively. They attributed the pre-described increase to rise in the number of dye molecules adsorbed on the photocatalyst [2] and the increased number of photons absorbed by the photocatalyst [31]. Dhatshanamurthi et al. [2] also explained that increased opacity of the solution at higher photocatalyst concentrations reduced the light penetration into the samples and resulted in lower decolorization efficiencies. Yang et al. [17] similarly explained that there is an optimal amount of photocatalyst which can make the maximum use of photo energy.

3.2.4. Effect of oxygen peroxide as an external electron acceptor

In the next step of the study in addition to the m-BVG, hydrogen peroxide (H_2O_2) was also used as an external electron acceptor with the aim of improving the decolorization rate. As depicted in Fig. 7, H_2O_2 addition at a content of 2 wt.% in conjunction with 1,400 mg/L m-BVG dramatically influenced the decolorization rate and resulted in 98% MO decolorization over 10 min of irradiation merely. This result is in line with those reported by Georgiou et al. [32] who used UV/H_2O_2 for degradation of azo-reactive dyes. They explained that complete destruction of the color was succeeded in the first 20–30 min of irradiation. This represents a relative high reaction rate of H_2O_2. Other researchers have also reported significant performance enhancements by the use of substances such as peroxomonosulphate and hydrogen peroxide [31]. They ascribed it to the generation of enhanced number of surface active radicals by reaction between electron acceptors and the photocatalyst.

To have a better insight into the H_2O_2/m-BVG composite performance, decolorization performance of H_2O_2 was examined solely. According to the results, it took about 60 min for H_2O_2 to reach the same decolorization efficiency (i.e., about 98%) under visible light irradiation. Considering the individual decolorization curves of m-BVG and H_2O_2, it can be realized that the sum of their decolorization efficiency at the 40th min of the process did not exceed 40%. Therefore, such an enhancement of the color removal rate using H_2O_2/m-BVG composite can be explained as a synergy phenomenon in which some of the photocatalytic mechanisms are accelerated or some new ones propagated. This subject is discussed more in section 3.3.

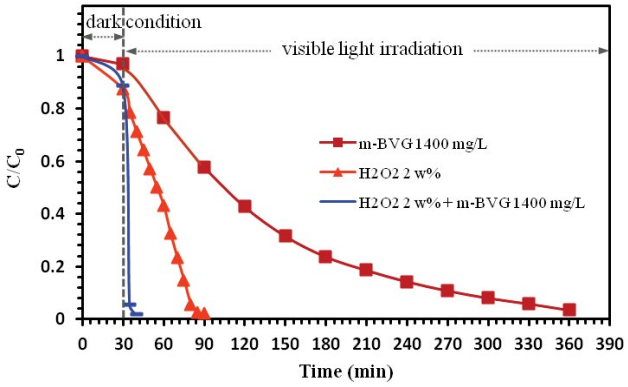

Fig. 7. Decolorization performance of m-BVG, H_2O_2 and H_2O_2/m-BVG.

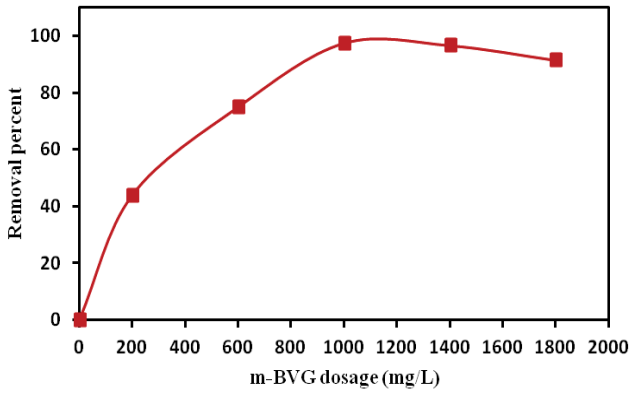

Fig. 6. Decolorization efficiency of different m-BVG dosages at 330th min of irradiation.

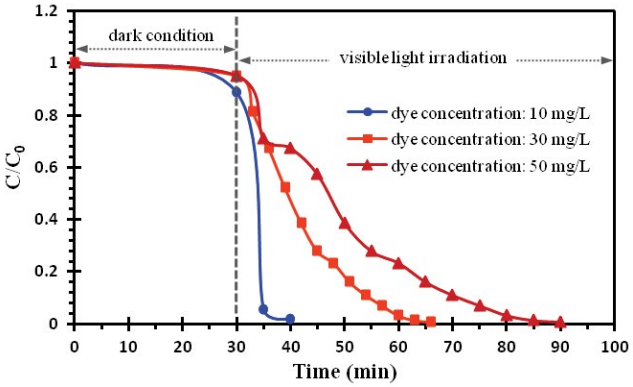

Fig. 8. Effect of the initial dye concentration on decolorization performance of H_2O_2/m-BVG (H_2O_2: 2wt.%, m-BVG: 1,400 mg/L).

3.2.5. Effect of initial dye concentration

Experiments were carried out to investigate the influence of initial dye concentration on the decolorization efficiency of the H_2O_2/m-BVG composite. According to the obtained results (Fig. 8), the initial dye concentration severely influenced the decolorization rates so that almost complete decolorization efficiency was obtained over only 10 min irradiation for the dye concentration of 10 mg/L, while it was achieved after about 35 and 60 min irradiation for the dye concentrations of 30 and 50 mg/L, respectively. The rapid decrease and complete disappearance of the main absorption peak of the MO at concentration of 50 mg/L during the photocatalytic reaction using H_2O_2/m-BVG is illustrated in Fig. 9.

As the light penetration into the mixture declines with increase of dye concentration, longer irradiation times were required for complete decolorization at higher MO concentrations. Ai et al. [33] reported lower dye removal efficiency at the dye concentrations of more than 10 mg/L. However, for the dye concentrations below 10 mg/L, Ai et al. [33] observed a slight enhancement in decolorization performance with increasing of the initial dye concentration. This may imply that below a certain amount of dye concentration, the decolorization rate essentially depends on the proper and sufficient contact between oxidizing species and dye molecules, while beyond that specific amount, the solution permeability to light will be the predominant controlling factor.

3.3. Involved photocatalytic mechanisms

Under the visible light irradiation, the valence electrons of $BiVO_4$ became excited and began to migrate from the valence band to the conduction band. This action produced the electron–hole pairs which intrinsically tend to recombine. Owing to high electrical conductivity, the graphene particles in the m-BVG composite, acted as an electron acceptor and helped to keep holes and valance electrons more steadily at an appropriate distance. This indeed reduced the recombination rate of photogenerated electron–hole pairs and resulted in better decolorization performance of m-BVG compared with the $BiVO_4$.

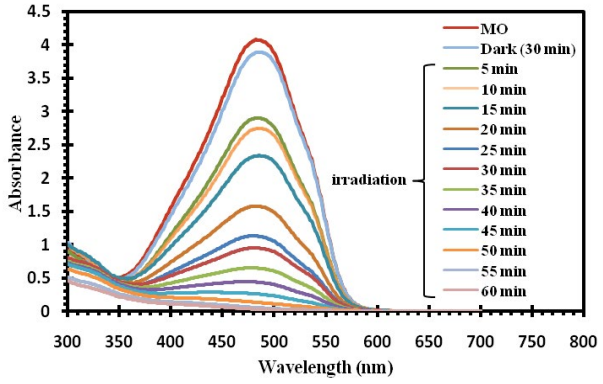

Fig. 9. Changes of absorbance spectra of MO as a function of irradiation time using H_2O_2/m-BVG (MO concentration: 50 mg/L, H_2O_2: 2 wt.%, m-BVG: 1,400 mg/L).

Considering the previous reports on the possible photocatalytic reactions involved in production of free radical species (Eqs. (1)–(9)) [7,12,32,34], the following reactions would be suggested for H_2O_2/m-BVG composite:

$$BiVO_4 + h\nu \rightarrow BiVO_4(h^+_{VB}) + BiVO_4(e^-_{CB}) \quad (1)$$

$$H_2O + h^+_{VB} \rightarrow OH^\bullet + H^+ \quad (2)$$

$$O_2 + e^-_{CB} \rightarrow {}^\bullet O_2^- \quad (3)$$

$${}^\bullet O_2^- + H^+ \rightarrow {}^\bullet OOH \quad (4)$$

$${}^\bullet OOH + {}^\bullet OOH \rightarrow H_2O_2 + O_2 \text{ and/or } {}^\bullet O_2^- + e^-_{CB} + 2H^+ \rightarrow H_2O_2 \quad (5)$$

$$H_2O_2 + e^-_{CB} \rightarrow OH^\bullet + OH^- \quad (6)$$

$$H_2O_2 + {}^\bullet O_2^- \rightarrow OH^\bullet + OH^- + O_2 \quad (7)$$

$$OH^- + h^+_{VB} \rightarrow OH^\bullet \quad (8)$$

$$H_2O_2 + h\nu \rightarrow 2OH^\bullet \quad (9)$$

From the above equations, it is clear that without using H_2O_2 as an external electron acceptor, the long pathway from Eq. (1) to Eq. (5) is required for occurrence of the next four reactions and generation of more $OH^\cdot$ radicals, which are highly powerful oxidizing species. In fact, addition of H_2O_2 to the mixture has resulted in elimination of the necessity of going through Eqs. (1)–(5) as a pre-required condition, and the reactions 6 to 9 could happen independently and directly. This accelerates the generation of $OH^\cdot$ species and dramatically enhances the decolorization rate of H_2O_2/m-BVG composite. Zhang et al. [35], who investigated the photocatalytic disinfection of *E. coli* K-12 by using an AgBr-Ag-Bi_2WO_6 nanojunction system under visible light irradiation, explained that the hydroxyl radicals ($OH^\cdot$) played most important role in the disinfection process. However, according to Ma et al. [36], who used C70 modified BiOCl photocatalyst, superoxide radicals (O_2^-) and holes (h^+_{VB}) were the main active species during the photocatalytic degradation of rhodamine B. Obviously, many structural, chemical and operational factors could impact on a certain photocatalyst performance in terms of generation of reactive species and overall oxidative ability.

3.4. Comparison with other studies

To have a comparison between the results obtained in the present study and other researches in the field of dye decolorization and removal with the use of photocatalysis process, some data are summarized in Table 1. In spite of the diversity of the values taken by the researchers for different experimental parameters (e.g., photocatalyst dosage, dye concentration, sample volume, light source and its power, etc.) it can be barely said that the m-BVG had a better performance than the other photocatalysts in the list. However, the m-BVG/H_2O_2 composite clearly performed superior in comparison with the others.

Table 1
Data of decolorization performance of different photocatalysts according to the present and some recent studies

Photocatalyst type	Photocatalyst dosage (g/L)	Dye	Dye concentration (mg/L)	Sample volume (ml)	Light source (W)	Time of irradiation (min)	Removal/ decolorization efficiency (%)	Reference
GO/TiO_2	1	MO	10	100	Visible (400)	180	65	[37]
GO/TiO_2							52	
ZnO/W	0.16	Ponceau 4R	20	500	UV	60	60	[38]
MnCo–Ferrite/TiO_2	0.5	MO	10	200	UV (400)	180	73	[39]
		MB[a]	14				99	
		CR[b]	10				99	
TiO_2-Silica	0.8	Reactive Blue 19	25	250	UV (150)	240	97.9	[40]
H_2O_2	30 wt.%	Five azo dyes	100	4000	UV (120)	120	100	[32]
GO/ZnO	0.04	MB	20	10	UV	180	70	[41]
$BiVO_4$/CeO_2	1	MO	7.5	50	Visible	30	80	[42]
ZnO/CuO	1	MO	3.0	500	UV	120	87	[12]
GO/TiO_2	0.6	MO	10	50	Visible (450)	240	70	[10]
TGSP[c]						180	100	
GO/BiOI	1	MO	3.3	50	Visible (200)	120	67	[43]
m-BVG	1.4	MO	10	50	Visible (40)	180	78	Present study
						240	82	
H_2O_2	2 wt.%					60	100	
m-BVG/H_2O_2	1.4/2 wt.%					10	100	

[a]Methylene Blue.
[b]Congo Red.
[c]Tin porphyrin-pillared GO-TiO_2 composite.

4. Conclusion

GO- and bismuth-based photocatalysts including $BiVO_4$, BVG, m-BVG and H_2O_2/m-BVG were synthesized and examined for the color removal from aqueous solution containing azo dye methyl orange (MO). GO exhibited a decreasing adsorption rate with time as its performance significantly depended on the remained available adsorption sites on GO sheets and the number of effective collisions between reactant molecules and particles. The decolorization rates that were observed for $BiVO_4$, BVG and particularly m-BVG were steadier in comparison with GO. This could indicate their strong photocatalytic activity which lets them to perform less dependent on the dye concentration. Comparing the synthesized $BiVO_4$ and BVG, the synthesized m-BVG exhibited higher decolorization rate and efficiency at any given time of the test. The m-BVG performance was predominantly controlled by the solution permeability to light as a function of both m-BVG dosage and dye concentration. The synergistic performance of H_2O_2/m-BVG composite resulted in around 98% MO decolorization over only 10 min of irradiation, while it lasted about 330 and 60 min for m-BVG and H_2O_2, respectively, to gain the same decolorization efficiency.

Acknowledgments

The authors gratefully acknowledge the Iran University of Science and Technology (IUST) for providing the research materials and equipments and supporting financially. Dr. Solmaz Zargari is also acknowledged for her kind assistance during the work.

References

[1] Y. Çalışkan, H.C. Yatmaz, N. Bektaş, Photocatalytic oxidation of high concentrated dye solutions enhanced by hydrodynamic cavitation in a pilot reactor, Process Saf. Environ., 111 (2017) 428–438.
[2] P. Dhatshanamurthi, M. Shanthi, M. Swaminathan, An efficient pilot scale solar treatment method for dye industry effluent using nano-ZnO, J. Water Process Eng., 16 (2017) 28–34.
[3] R. Croce, F. Cinà, A. Lombardo, G. Crispeyn, C.I. Cappelli, M. Vian, S. Maiorana, E. Benfenati, D. Baderna, Aquatic toxicity of several textile dye formulations: Acute and chronic assays with Daphnia magna and Raphidocelis subcapitata, Ecotoxicol. Environ. Saf., 144 (2017) 79–87.
[4] O.M. Min, L.N. Ho, S.A. Ong, Y.S. Wong, Comparison between the photocatalytic degradation of single and binary azo dyes in TiO_2 suspensions under solar light irradiation, J. Water Reuse Desalin. 5 (2015) 579–591.
[5] A. Reife, H.S. Freeman, Environmental Chemistry of Dyes and Pigments, Wiley, New York, 1996.
[6] J. Fenoll, P. Flores, P. Hellín, C.M. Martínez, S. Navarro, Photodegradation of eight miscellaneous pesticides in drinking water after treatment with semiconductor materials under sunlight at pilot plant scale, Chem. Eng. J., 204–206 (2012) 54–64.
[7] H. Zangeneh, A.A.L. Zinatizadeh, M. Habibi, M. Akia, M.H. Isa, Photocatalytic oxidation of organic dyes and pollutants in wastewater using different modified titanium dioxides: a comparative review, J. Ind. Eng. Chem., 26 (2015) 1–36.
[8] R. Rahimi, S. Zargari, A. Yousefi, M. Yaghoubi Berijani, A. Ghaffarinejad, A. Morsali, Visible light photocatalytic disinfection of E. coli with TiO_2–graphene nanocomposite sensitized with tetrakis(4-carboxyphenyl)porphyrin, Appl. Surf. Sci., 355 (2015) 1098–1106.
[9] C. Ravidhas, A. Juliat Josephine, P. Sudhagar, A. Devadoss, C. Terashima, K. Nakata, A. Fujishima, A. Moses Ezhil Raj, C. Sanjeeviraja, Facile synthesis of nanostructured monoclinic bismuth vanadate by a co-precipitation method: Structural, optical and photocatalytic properties, Mater. Sci. Semicond. Proc., 30 (2015) 343–351.
[10] S. Zargari, R. Rahimi, A. Ghaffarinejad, A. Morsali, Enhanced visible light photocurrent response and photodegradation efficiency over TiO_2-graphene nanocomposite pillared with tin porphyrin, J. Colloid Interface Sci., 466 (2016) 310–321.
[11] Y. Geng, P. Zhang, N. Li, Z. Sun, Synthesis of Co doped $BiVO_4$ with enhanced visible-light photocatalytic activities, J. Alloys Compd., 651 (2015) 744–748.
[12] R. Saravanan, S. Karthikeyan, V.K. Gupta, G. Sekaran, V. Narayanan, A. Stephen, Enhanced photocatalytic activity of ZnO/CuO nanocomposite for the degradation of textile dye on visible light illumination, Mater. Sci. Eng.: C, 33 (2013) 91–98.
[13] C. Adán, J. Marugán, S. Obregón, G. Colón, Photocatalytic activity of bismuth vanadates under UV-A and visible light irradiation: Inactivation of Escherichia coli vs oxidation of methanol, Catal. Today, 240 (2015) 93–99.
[14] H.B. Li, J. Zhang, G.Y. Huang, S.H. Fu, C. Ma, B.Y. Wang, Q.R. Huang, H.W. Liao, Hydrothermal synthesis and enhanced photocatalytic activity of hierarchical flower-like Fe-doped $BiVO_4$, Trans Nonferrous Metal Soc., 27 (2017) 868–875.
[15]C. Zhou, P. Xu, C. Lai, C. Zhang, G. Zeng, D. Huang, M. Cheng, L. Hu, W. Xiong, X. Wen, L. Qin, J. Yuan, W. Wang, Rational design of graphic carbon nitride copolymers by molecular doping for visible-light-driven degradation of aqueous sulfamethazine and hydrogen evolution, Chem. Eng. J., 359 (2019) 186–196.
[16] X. Meng, Z. Zhang, Bismuth-based photocatalytic semiconductors: Introduction, challenges and possible approaches, J. Mol. Catal. A, 423 (2016) 533–549.
[17] Y. Yang, Z. Zeng, C. Zhang, D. Huang, G. Zeng, R. Xiao, C. Lai, C. Zhou, H. Guo, W. Xue, M. Cheng, W. Wang, J. Wang, Construction of iodine vacancy-rich BiOI/Ag@AgI Z-scheme heterojunction photocatalysts for visible-light-driven tetracycline degradation: transformation pathways and mechanism insight, Chem. Eng. J., 349 (2018) 808–821.
[18] Y. Yang, C. Zhang, C. Lai, G. Zeng, D. Huang, M. Cheng, J. Wang, F. Chen, C. Zhou, W. Xiong, BiOX(X=Cl, Br, I) photocatalytic nanomaterials: applications for fuels and environmental management, Adv. Colloid Interface Sci., 254 (2018) 76–93.
[19] L. Shan, J. Bi, C. Lu, Y. Xiao, $BiVO_4$(010)/rGO nanocomposite and its photocatalysis application, J. Inorg. Organomet. Polym., 29 (2019) 1000–1009.
[20] L. Shan, G. Wang, J. Suriyaprakash, D. Li, L. Liu, L. Dong, Solar light driven pure water splitting of B-doped $BiVO_4$ synthesized via a sol-gel method, J. Alloys Compd., 636 (2015) 131–137.
[21] L. Ge, Novel Pd/$BiVO_4$ composite photocatalysts for efficient degradation of methyl orange under visible light irradiation, Mater. Chem. Phys., 107 (2008) 465–470.
[22] L. Shan, Y. Liu, C. Ma, L. Dong, L. Liu, Z. Wu, Enhanced photocatalytic performance in Ag^+-induced $BiVO_4$/β-Bi_2O_3 heterojunctions, Eur. J. Inorg. Chem., 2 (2016) 232–239.
[23] B. Zhou, X. Zhao, H.J. Liu, J.H. Qu, C.P. Huang, Synthesis of visible-light sensitive M-$BiVO_4$ (M=Ag, Co, and Ni) for the photocatalytic degradation of organic pollutants, Sep. Purif. Technol., 77 (2011) 275–282.
[24] S.H. Hsieh, J.M. Ting, Characterization and photocatalytic performance of ternary Cu-doped ZnO/graphene materials, Appl. Surf. Sci., 427 (2018) 465–475.
[25] H.N. Tien, V.H. Luan, L.T. Hoa, N.T. Khoa, S.H. Hahn, J.S. Chung, E.W. Shin, S.H. Hur, One-pot synthesis of a reduced graphene oxide-zinc oxide sphere composite and its use as a visible light photocatalyst, Chem. Eng. J., 229 (2013) 126–133.
[26] T. Wang, C. Li, J. Ji, Y. Wei, P. Zhang, S. Wang, X. Fan, J. Gong, Reduced graphene oxide (rGO)/$BiVO_4$ composites with maximized interfacial coupling for visible light photocatalysis, ACS Sustain. Chem. Eng., 2 (2014) 2253–2258.
[27] W.S. Hummers Jr., R.E. Offeman, Preparation of graphitic oxide, J. Am. Chem. Soc., 80 (1958) 1339–1339.
[28] C. Karunakaran, S. Kalaivani, P. Vinayagamoorthy, S. Dash, Electrical, optical and visible light-photocatalytic properties of

monoclinic $BiVO_4$ nanoparticles synthesized hydrothermally at different pH, Mater. Sci. Semicond. Proc., 21 (2014) 122–131.
[29] W. Peng, H. Li, Y. Liu, S. Song, A review on heavy metal ions adsorption from water by graphene oxide and its composites, J. Mol. Liq., 230 (2017) 496–504.
[30] T. Xu, L. Zhang, H. Cheng, Y. Zhu, Significantly enhanced photocatalytic performance of ZnO via graphene hybridization and the mechanism study, Appl. Catal., B, 101 (2011) 382–387.
[31] P. Sathishkumar, R. Sweena, J.J. Wu, S. Anandan, Synthesis of CuO-ZnO nanophotocatalyst for visible light assisted degradation of a textile dye in aqueous solution, Chem. Eng. J., 171 (2011) 136–140.
[32] D. Georgiou, P. Melidis, A. Aivasidis, K. Gimouhopoulos, Degradation of azo-reactive dyes by ultraviolet radiation in the presence of hydrogen peroxide, Dyes Pigm., 52 (2002) 69–78.
[33] L. Ai, C. Zhang, L. Li, J. Jiang, Iron terephthalate metal–organic framework: revealing the effective activation of hydrogen peroxide for the degradation of organic dye under visible light irradiation, Appl. Catal., B, 148–149 (2014) 191–200.
[34] Y. Yang, C. Zhang, D. Huang, G. Zeng, J. Huang, C. Lai, C. Zhou, W. Wang, H. Guo, W. Xue, R. Deng, M. Cheng, W. Xiong, Boron nitride quantum dots decorated ultrathin porous g-C_3N_4: intensified exciton dissociation and charge transfer for promoting visible-light-driven molecular oxygen activation, Appl. Catal., B, 245 (2019) 87–99.
[35] L.S. Zhang, K.H. Wong, H.Y. Yip, C. Hu, J.C. Yu, C.Y. Chan, P.K. Wong, Effective photocatalytic disinfection of *E. coli* K-12 using AgBr–Ag–Bi_2WO_6 nanojunction system irradiated by visible light: the role of diffusing hydroxyl radicals, Environ. Sci. Technol., 44 (2010) 1392–1398.
[36] D. Ma, J. Zhong, J. Li, L. Wang, R. Peng, Enhanced photocatalytic activity of BiOCl by C70 modification and mechanism insight, Appl. Surf. Sci., 443 (2018) 497–505.
[37] N.R. Khalid, E. Ahmed, Z. Hong, L. Sana, M. Ahmed, Enhanced photocatalytic activity of graphene-TiO_2 composite under visible light irradiation, Curr. Appl. Phys., 13 (2013) 659–663.
[38] M. Vafaee, M.E. Olya, J.Y. Drean, A.H. Hekmati, Synthesize, characterization and application of ZnO/W/Ag as a new nanophotocatalyst for dye removal of textile wastewater; kinetic and economic studies, J. Taiwan Inst. Chem. Eng., 80 (2017) 379–390.
[39] S. Yousefi-Mohammadi, M. Movahedi, H. Salavati, MnCo–Ferrite/TiO_2 composite as an efficient magnetically separable photocatalyst for decolorization of dye pollutants in aqueous solution, Surf. Interfaces, 11 (2018) 91–97.
[40] D. Maučec, A. Šuligoj, A. Ristić, G. Dražić, A. Pintar, N.T. Novak, Titania versus zinc oxide nanoparticles on mesoporous silica supports as photocatalysts for removal of dyes from wastewater at neutral pH, Catal. Today, 310 (2018) 32–41.
[41] T. Kavitha, A.I. Gopalan, K.P. Lee, S.Y. Park, Glucose sensing, photocatalytic and antibacterial properties of graphene-ZnO nanoparticle hybrids, Carbon, 50 (2012) 2994–3000.
[42] N. Wetchakun, S. Chaiwichain, B. Inceesungvorn, K. Pingmuang, S. Phanichphant, A.I. Minett, J. Chen, $BiVO_4$/CeO_2 nanocomposites with high visible-light-induced photocatalytic activity, ACS appl. Mater. Interfaces, 4 (2012) 3718–3723.
[43] F.J. Zhang, F.Z. Xie, W.J. Xie, C.X. Zhu, Graphene/BiOI Composites synthesized via the oil bath method and their application for efficient photocatalytic degradation of Methyl Orange under visible light irradiation, Kinet. Catal., 57 (2016) 339–343.